Research Article Vol. 6, No. 4 / April 2019 / Optica 460

Blind ghost imaging

Alba M. Paniagua-Diaz,[1,†] Ilya Starshynov,[1,†] Nikos Fayard,[2,†] Arthur Goetschy,[2] Romain Pierrat,[2] Rémi Carminati,[2] and Jacopo Bertolotti[1,*]

[1]University of Exeter, Stocker Road, Exeter EX4 4QL, UK
[2]ESPCI Paris, PSL Research University, CNRS, Institut Langevin, 1 rue Jussieu, F-75005, Paris, France
*Corresponding author: j.bertolotti@exeter.ac.uk

Received 4 December 2018; revised 6 March 2019; accepted 9 March 2019 (Doc. ID 352420); published 9 April 2019

Ghost imaging is an unconventional optical imaging technique that reconstructs the shape of an object by combining the measurement of two signals: one that interacted with the object, but without any spatial information; the other containing spatial information, but that never interacted with the object. Here we demonstrate that ghost imaging can be performed without ever knowing the patterns that illuminate the object, by instead using patterns correlated with them, no matter how weakly. As an experimental proof, we reconstruct the image of an object hidden behind a scattering layer using only the reflected light, which never interacts with the object.

https://doi.org/10.1364/OPTICA.6.000460

1. INTRODUCTION

In its simplest form ghost imaging (GI) is an imaging technique closely related to dual photography [1] and single pixel camera [2] where, instead of uniformly illuminating an object and then detecting the scattered light with a multipixel camera, the object is illuminated with a sequence of known patterns and the scattered light is detected by a single photodiode [3,4]. By using enough illumination patterns, high-quality images can be formed [5]. Ghost imaging is a very flexible technique that has been generalized to the single-photon regime [6], to the time domain [7], to infrared and terahertz frequencies [8], and to many more conditions [9]. Since there is a lot of freedom in the choice of the patterns used, one can optimize them to increase resolution in the areas of interest [10], or use compressive sensing to speed-up measurement [11]. Furthermore, as long as the patterns used are known, they do not need to be deterministically generated or even orthogonal; even a set of speckle patterns allow the reconstruction of an image [12].

A property shared by all variants of ghost imaging is that the exact set of illumination patterns must be known. What is effectively measured with a single pixel detector is proportional to the overlap between the object O and the illumination pattern P_i (i.e., the coefficient $b_i = \int P_i(\boldsymbol{r})O(\boldsymbol{r})\mathrm{d}\boldsymbol{r}$). If the set of illumination patterns forms a complete basis, one can reconstruct an image of the object as $I(\boldsymbol{r}') = \sum_i b_i P_i(\boldsymbol{r}')$. However, if the patterns P_i are unknown, this approach breaks down.

In this paper we show that even if the illumination patterns are completely unknown it is possible to use a different set of patterns in the reconstruction formula, as long as this second set is correlated with the first one. In particular, we exploit the recently discovered spatial correlation between the transmitted and reflected speckle patterns generated at both sides of a scattering medium [13,14], which allows us to reconstruct the shape of an object hidden behind a turbid medium, potentially fully opaque, using only the reflected speckle pattern rather than the transmitted one. Furthermore, we generalize this technique to a completely noninvasive geometry, where both the camera measuring the speckle pattern and the single-pixel detector are on the same side of the scattering layer, which allows us to image a fluorescent object placed on the other side.

2. METHOD

When using speckle to perform ghost imaging, one usually sends a laser beam through a time-varying scattering medium, often a rotating diffuser, and the resulting transmitted intensity speckle pattern, T_i, is measured and used as the illumination pattern P_i. The transmitted light passing through the object is then integrated and measured with a single pixel detector, yielding the coefficient $b_i = \int T_i(\boldsymbol{r})O(\boldsymbol{r})\mathrm{d}\boldsymbol{r}$. Full knowledge of both b_i and T_i allows one to obtain a faithful representation of the object O, for a large enough number N of patterns. To measure directly the transmitted speckle patterns, one must have an imaging system placed behind the scattering layer. In most practical situations, this arrangement is actually not possible (e.g., because access is restricted, as in biomedical imaging). In these cases, one can rely on the reflected speckle patterns R_i only, which share mutual information with the transmitted ones in the form of a spatial correlation [13–15]. The simplest approach to make use of this mutual information is to replace each $T_i(\boldsymbol{r}')$ with $R_i(\boldsymbol{r}')$, which results in the reconstructed image,

$$\tilde{I}(\boldsymbol{r}') = \sum_{i=1}^{N} b_i R_i(\boldsymbol{r}'). \quad (1)$$

Identifying the sum $\sum_{i=1}^{N}(\ldots)_i$ with the ensemble average $\langle\ldots\rangle$ and substituting in the definition of b_i, we can express the reconstructed image as

$$\begin{aligned}\tilde{I}(\boldsymbol{r}') &= \left\langle \int O(\boldsymbol{r})T(\boldsymbol{r})R(\boldsymbol{r}')\mathrm{d}\boldsymbol{r} \right\rangle \\ &= \int O(\boldsymbol{r})\langle T(\boldsymbol{r})R(\boldsymbol{r}')\rangle \mathrm{d}\boldsymbol{r} \\ &= \langle T\rangle\langle R\rangle \left[O * C^{RT} + \int O(\boldsymbol{r})\mathrm{d}\boldsymbol{r} \right] \\ &\propto O * C^{\mathrm{RT}} + \mathcal{A}, \end{aligned} \quad (2)$$

where $C^{\mathrm{RT}}(\Delta\boldsymbol{r}) = \langle \delta R(\boldsymbol{r})\delta T(\mathbf{r}+\Delta\boldsymbol{r})\rangle$ is the normalized correlation function of the reflected and transmitted intensity patterns ($\delta f = f/\langle f\rangle - 1$ denotes the normalized statistical fluctuation of the random variable f) and the constant $\mathcal{A} = \int O(\boldsymbol{r})\mathrm{d}\boldsymbol{r}$ represents a flat background proportional to the total signal from the object. Hence, using the reflected speckle patterns instead of the transmitted ones, we obtain the very same image, but with a lower resolution given by the range of the correlation function C^{RT}, which acts as a point spread function. We name this approach blind ghost imaging (BGI), as it allows one to perform ghost imaging without ever knowing the patterns used to illuminate the object.

3. RESULTS

A. Blind Ghost Imaging

To verify our prediction we designed an experiment where we image an object hidden behind an opaque scattering medium. The experimental apparatus is shown in Fig. 1(a). A 2 mW He–Ne laser is incident on a scattering medium [Fig. 1(a), inset]

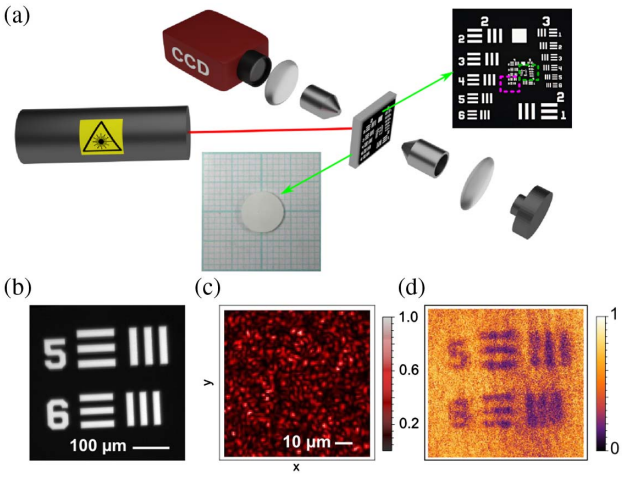

Fig. 1. (a) Experimental apparatus. A cw laser illuminates an opaque scattering material and an object hidden behind (insets). An imaging system records the reflected speckle pattern from the surface of the scattering sample and a bucket detector collects the intensity transmitted by the object. (b) Elements 5 and 6 of Group 4 of the resolution target used as object to image in this experiment, highlighted by the pink square in the inset of panel (a). (c) Typical speckle pattern collected in reflection with the imaging system presented. (d) Retrieved image using BGI with 2.27×10^6 disorder realizations.

at an angle of approximately 45° with respect to the sample surface. In this way, contributions of the specularly reflected and ballistically transmitted light, which spoil the correlation C^{RT}, are not collected [14]. The scattering layer is made of a suspension of TiO_2 particles in glycerol with a concentration of 300 mg of TiO_2 for 10 mL of glycerol, which leads to a scattering mean free path $\ell = 16 \pm 2$ μm. The suspension is held between one glass slide and the resolution target that works as the object to image, and its thickness is controlled using calibrated feeler gauges. Throughout the experiments described here we used a fixed $L = 40$ μm thickness. These parameters result in an optical density (OD) $L/\ell \simeq 2.5$. The object to image, a Thorlabs USAF 1951 calibration test target [Fig. 1(b)], is in contact with the scattering layer. The reflected speckle pattern [Fig. 1(c)] is imaged on the scattering medium surface and recorded using a CCD camera. As the scattering layer is liquid, the speckle patterns change with time, which allows us to record a large number of different speckle patterns without moving or changing the sample. Due to the viscosity of glycerol, which causes slow movement of the particles, we use a piezoelectric buzzer attached to the glass slide holding the sample to speed up the movement of the particles and shorten the decorrelation time of the generated speckle patterns, which allows us to record different speckle patterns at the maximal acquisition speed of the cameras (around 17 frames per second), and perform an ensemble average. The transmitted light passing through the object is then integrated by a bucket detector. For simplicity of alignment, this is done using an identical CCD camera and integrating over all pixels. This action allows us to measure the correlation $C^{\mathrm{RT}}(\Delta\boldsymbol{r})$, discussed later, using the same apparatus.

In Fig. 1(d) we show the reconstructed image of the object represented in Fig. 1(b), when using the reflected speckle patterns and integrating the transmitted intensity, according to Eq. (1). Here, we used $N = 2.27 \times 10^6$ realizations of the disorder. Apart from the residual noise, the object is clearly visible and all features are resolved. We notice that a Gaussian smoothing of the picture would remove most of the noise, producing a more pleasing image. This experiment demonstrates that it is possible to perform ghost imaging using a set of patterns different from the illuminating one but correlated with it. In particular, it is possible to use the reflected, instead of the transmitted speckle, to reconstruct the shape of an object placed behind an opaque scattering layer. Compared to other ghost imaging schemes using reflected signal [16,17], this method works in the deep multiple scattering regime without using any ballistic light.

B. Noninvasive BGI

As the bucket detector does not have any spatial resolution, there is no fundamental reason why it should be placed behind the object as in traditional ghost imaging. This suggests that BGI can be adapted to a completely noninvasive configuration. We modified the apparatus so that all optical components are on the opposite side of the scattering layer with respect to the object, as shown in Fig. 2(a). The fluorescent sample consists of the USAF negative target with a fluorescent layer of cerium-doped YAG just behind it. The illumination geometry is the same as in the first experiment, but in this case we used a 100 mW blue laser (450 nm) producing a white fluorescent emission from the cerium-doped YAG layer. Both the reflected speckle and the fluorescence are collected by a 10x microscope objective, and a plano-convex 150 mm lens, in an epi configuration. The speckle pattern is

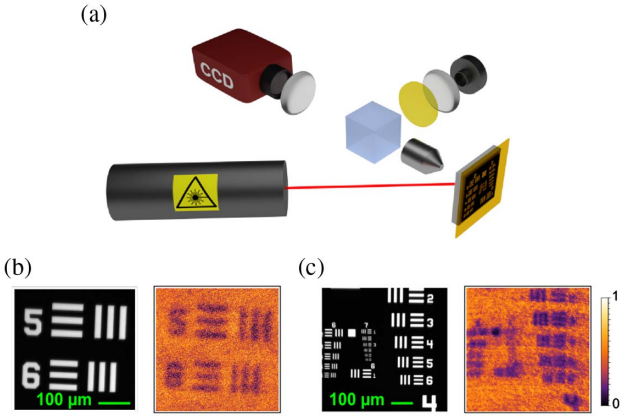

Fig. 2. (a) Experimental apparatus used for noninvasive BGI. A 450 nm laser is incident on the scattering sample at ≈45°. The resolution target is placed on the back surface of the scattering material, and right behind it we have a fluorescent layer (cerium-doped YAG), acting as a fluorescent object. The bucket detector is in this case also in reflection from the sample, filtering the fluorescent light with a 500 nm long pass filter. (b) Elements 5 and 6 of Group 4 of the resolution target used as the object, and the image retrieved using BGI with 4×10^6 disorder realizations. (c) Object representing Groups 5, 6, and 7 from the resolution target, and the image retrieved using BGI with 1.5×10^6 disorder realizations.

recorded by a CCD camera, and the fluorescence from the object is collected by the bucket detector after passing through a long-pass 500 nm filter. Again in this case the bucket detector is a CCD with the intensity integrated over all pixels. In Fig. 2(b) we show the retrieved image for this case, obtained with $N = 4 \times 10^6$ disorder realizations. The image is very well reconstructed, with an outcome very similar to the one shown in Fig. 1(d), obtained with the bucket placed on the transmission side.

C. BGI Performance

To evaluate the performance of the BGI setup, we first took an image of the elements 5 and 6 of Group 4 of the USAF target, as shown in Fig. 2(b), and found a lateral resolution $\Delta r \simeq 20$ μm. We then repeated the measurement with an object with smaller features (Groups 5, 6, and 7 of the resolution target) shown in Fig. 2(c), to better quantify the resolution of this method. According to our prediction [Eq. (2)], this resolution should be given by the width of the correlation $C^{\mathrm{RT}}(\boldsymbol{\Delta r})$ which acts as a point spread function. To confirm that this is indeed the case, we made a separate measurement of the average intensity correlation between transmitted and reflected speckle patterns [14]. We then compared the BGI results of Figs. 2(b) and 2(c) with the numerical convolution of the object with C^{RT}. The results are presented in Fig. 3. The retrieved images [Figs. 3(b) and 3(c)] resemble very well the expected ones [Figs. 2(b) and 2(c)], resolving the same elements and thus demonstrating that the resolution of the resulting image depends on the width and shape of the correlation function C^{RT} [Fig. 3(a)], as dictated by Eq. (2). In particular, the width of the correlation function limits the features of the object that can be resolved, even in the ideal and noise-free case, where it is possible to resolve mainly the first few elements of Group 5. The excellent agreement between the reconstructed images in Figs. 3(b) and 3(c), and the experimental images in Figs. 2(b) and 2(c), also proves that the image formation process in BGI does not rely on an information on the object directly

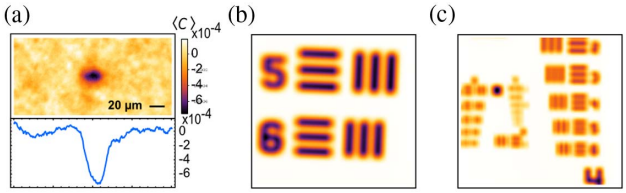

Fig. 3. (a) Two-dimensional (2D) map and a 1D cross section along $\Delta y = 0$ of the averaged correlation between the transmitted and reflected speckle patterns. (b) and (c) Expected images obtained by numerically convolving the objects shown in Figs. 2(b) and 2(c) with the correlation function shown in (a).

encoded in the reflected speckle pattern (since the correlation function in Fig. 3(a) is recorded in the absence of the object).

The shape and the sign of the correlation C^{RT} depend both on the sample thickness L and the scattering mean free path ℓ in a non-trivial way [14]. However, in the multiple scattering regime ($L \gtrsim \ell$), it takes a simple form, mostly isotropic and negative, with a width $\sim L$, as shown in Fig. 3(a). The negative sign of the correlation is the reason why the images appear as a negative signal on top of a bright background. In addition, the width scaling can be understood from the microscopic scattering process responsible for the correlation [18–20]. Interference between scattered waves create a bulk speckle pattern inside the disordered medium, which acts as an ensemble of local fluctuating sources for diffusive transport [21–25]. Two diffusive paths generated by the same source and emerging on opposite sides of the sample are thus correlated [26,27]. Since diffusive paths explore a domain of transverse size bounded by L, the range of C^{RT} necessarily scales linearly with L. This means that the resolution of the BGI scheme is given by the depth of the target object. This spatial resolution is comparable to that obtained in diffuse optical imaging, which uses a CCD camera in transmission instead of a simple bucket detector [28].

Another specific feature of the BGI scheme is its signal-to-noise ratio (SNR), which depends on the amplitude and the range of the correlation C^{RT}, as well as the size of the illuminated object. As discussed above, C^{RT} has a width of order L and a small amplitude α, so that the useful signal [i.e., first term of Eq. (2)] is always smaller than the constant background $\mathcal{A}$. In addition, because of the Rayleigh-like statistics of the speckle patterns used to reconstruct the image, fluctuations are large and proportional to the full signal. This results in a SNR $\sim \sqrt{N}\alpha L^2/\mathcal{A}$ (see Supplement 1 for details). Typically, in our experiment $\alpha \sim 10^{-3}$, which imposes a number of measurements $N \gtrsim 10^6$ to get SNR $\gtrsim 1$. In the deep diffusive regime, $L \gg \ell$, which is not reached in our experiment, it is known that $\alpha \sim \lambda^2/L^2$ [14]. The fact that in the deep diffusive regime, the amplitude of the correlation C^{RT} is inversely proportional to its typical area leads to SNR$\sim \sqrt{N}\lambda^2/\mathcal{A}$, which strikingly does not depend either on the scattering strength or on the sample thickness. This analysis shows that BGI can, in principle, be used to take the image of an object hidden behind a fully opaque medium in the deep diffusive regime.

D. BGI for a Distant Object

In the experiments described above, the object to be imaged was placed right on the back of the scattering layer and the reflected

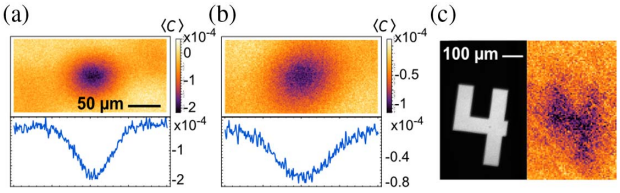

Fig. 4. (a) and (b) Correlation functions between the reflected and transmitted speckle patterns measured 80 μm and 160 μm, respectively, away from the transmission and reflection surfaces. (c) Object separated by a cover slip of 150 μm from the scattering medium and retrieved image using BGI with 5.65×10^5 disorder realizations.

speckle pattern was recorded at its front surface. In this configuration, C^{RT} is expected to be maximally peaked [14]. Since the latter originates from bulk speckle patterns, and thus from interference, we could wonder how C^{RT} is modified when the object is further away from the surface. As free space propagation preserves mutual information, the integral of $C^{\mathrm{RT}}(\Delta \boldsymbol{r})$ must be constant even when it is measured between two planes away from the scattering layer. At the same time, we expect that the mutual information will spread over larger and larger areas, until it becomes a constant function in the far field. To be more quantitative, we extended the theoretical analysis of [14] and computed analytically C^{RT} on two planes at arbitrary distances, D and D', away from the sample. We found that, in the regime $L \gg \ell$, one obtains the simple form $C^{\mathrm{RT}}(\Delta \boldsymbol{r}, D, D') = C^{\mathrm{RT}}(\Delta \boldsymbol{r}, 0, 0) * h(\Delta \boldsymbol{r}, D) * h(\Delta \boldsymbol{r}, D')$, where $h(\Delta \mathbf{r}, D)$ is a normalized function of width $\sim D$. This is confirmed by the results of extensive numerical simulations of the wave equation in a disordered slab illuminated with monochromatic light (see Supplement 1 for details). This means that objects located further away from the scattering layer can be imaged with almost unaffected resolution and contrast as long as $D, D' \ll L$. It also implies that the image quality does not depend on the exact position of the disordered sample, but rather on the distance between the object and the plane where the reflected speckle is imaged. To test these predictions, we measured the correlation C^{RT} from the same sample used in the previous experiments, on two planes placed at various distances from the sample. Representative results are shown in Figs. 4(a) and 4(b) for planes at 80 μm and 160 μm, respectively, away from the sample (see Supplement 1 for a systematic study). As can be seen, the correlation does become wider, but does so gradually. Hence, it is possible to use BGI to image objects away from the scattering layer at the price of a reduced resolution, but without introducing complicated aberrations. This is illustrated in Fig. 4(c), where we show an object and its BGI retrieved image, when the reflected speckle pattern was measured on the surface of the sample and the scattering medium is 150 μm away from the object. The number of measurements needed to retrieve that image was $N = 5.65 \times 10^5$. This experiment successively mimics a situation where one does not necessarily know how far away the object is from the scattering layer.

4. CONCLUSIONS

We have demonstrated ghost imaging through an opaque scattering medium without measuring the transmitted speckle pattern that illuminates the target. The BGI scheme instead uses a measurement of the reflected speckle that is merely spatially correlated with the transmitted one. The achievable resolution is given by the width of the correlation function, while the number of realizations of the disorder needed to obtain a noiseless image depends both on the amplitude of the correlation function and the total signal received by the bucket detector. Fundamentally, our results illustrate an important feature of ghost imaging; namely, that one does not need to measure the illuminating signal, but only a signal weakly correlated to it. Practically, this broadens the potential range of applications of ghost imaging, in particular for noninvasive imaging in biological tissues. Compared to other techniques, BGI has a resolution comparable to diffuse optical imaging, but its SNR becomes independent on the thickness and scattering mean free path in the diffusive limit. Other correlation-based imaging techniques allow the reconstruction of the shape of an object behind a scattering layer by exploiting the optical memory effect [18]. These techniques benefit from a resolution limited by the speckle grain size only, but they suffer from a limited field of view that tends to zero for an object close to the sample surface [29,30].

Several possible strategies can be used to improve the processing speed of BGI, which is limited by the large amount of measurements required to reach a viable SNR: Fast-moving scattering media in conjunction with fast cameras will naturally reduce measurement time. For slow-moving media, however, one can generate different (unknown) illumination patterns by modulating the incident wavefront with a spatial light modulator. Alternatively, compressive sensing techniques could reduce the number of necessary measurements, as long as some assumption (e.g., sparsity) can be made about the object to be imaged [11].

Funding. Engineering and Physical Sciences Research Council (EPSRC) (EP/L015331/1); LABEX WIFI (ANR-10-LABX-24, ANR-10-IDEX-0001-02 PSL*); Leverhulme Trust (PLP-2015-216); Direction Générale de l'Armement (DGA).

Acknowledgment. Leverhulme Trust's Philip Leverhulme Prize, and by LABEX WIFI (Laboratory of Excellence within the French Program, "Investments for the Future"). Authors Ilya Starshynov and Alba M. Paniagua-Diaz acknowledge support through the Centre of Doctoral Training in Metamaterials (XM^2). Author Nikos Fayard acknowledges financial support from the French "Direction Générale de l'Armement" (DGA). The research data supporting this publication are openly available from the University of Exeter's institutional repository at [31].

See Supplement 1 for supporting content.

†These authors contributed equally to this work.

REFERENCES

1. P. Sen, B. Chen, G. Garg, S. R. Marschner, M. Horowitz, M. Levoy, and H. P. A. Lensch, "Dual photography," ACM Trans. Graph. **24**, 745 (2005).
2. M. F. Duarte, M. A. Davenport, D. Takhar, J. N. Laska, T. Sun, K. F. Kelly, and R. G. Baraniuk, "Single-pixel imaging via compressive sampling," IEEE Signal Process. Mag. **25**, 83–91 (2008).
3. T. B. Pittman, Y. H. Shih, D. V. Strekalov, and A. V. Sergienko, "Optical imaging by means of two-photon quantum entanglement," Phys. Rev. A **52**, R3429–R3432 (1995).
4. R. S. Bennink, S. J. Bentley, and R. W. Boyd, "Two-photon coincidence imaging with a classical source," Phys. Rev. Lett. **89**, 113601 (2002).

5. F. Ferri, D. Magatti, A. Gatti, M. Bache, E. Brambilla, and L. A. Lugiato, "High-resolution ghost image and ghost diffraction experiments with thermal light," Phys. Rev. Lett. **94**, 183602 (2005).
6. R. S. Aspden, D. S. Tasca, R. W. Boyd, and M. J. Padgett, "EPR-based ghost imaging using a single-photon-sensitive camera," New J. Phys. **15**, 073032 (2013).
7. P. Ryczkowski, M. Barbier, A. T. Friberg, J. M. Dudley, and G. Genty, "Ghost imaging in the time domain," Nat. Photonics **10**, 167–170 (2016).
8. D. Shrekenhamer, C. M. Watts, and W. J. Padilla, "Terahertz single pixel imaging with an optically controlled dynamic spatial light modulator," Opt. Express **21**, 12507–12518 (2013).
9. M. J. Padgett and R. W. Boyd, "An introduction to ghost imaging: quantum and classical," Philos. Trans. R. Soc. A **375**, 20160233 (2017).
10. D. B. Phillips, M.-J. Sun, J. M. Taylor, M. P. Edgar, S. M. Barnett, G. M. Gibson, and M. J. Padgett, "Adaptive foveated single-pixel imaging with dynamic supersampling," Sci. Adv. **3**, e1601782 (2017).
11. O. Katz, Y. Bromberg, and Y. Silberberg, "Compressive ghost imaging," Appl. Phys. Lett. **95**, 131110 (2009).
12. P. Zerom, Z. Shi, M. N. O'Sullivan, K. W. C. Chan, M. Krogstad, J. H. Shapiro, and R. W. Boyd, "Thermal ghost imaging with averaged speckle patterns," Phys. Rev. A **86**, 063817 (2012).
13. N. Fayard, A. Cazé, R. Pierrat, and R. Carminati, "Intensity correlations between reflected and transmitted speckle patterns," Phys. Rev. A **92**, 033827 (2015).
14. I. Starshynov, A. M. Paniagua-Diaz, N. Fayard, A. Goetschy, R. Pierrat, R. Carminati, and J. Bertolotti, "Non-Gaussian correlations between reflected and transmitted intensity patterns emerging from opaque disordered media," Phys. Rev. X **8**, 021041 (2018).
15. N. Fayard, A. Goetschy, R. Pierrat, and R. Carminati, "Mutual information between reflected and transmitted speckle images," Phys. Rev. Lett. **120**, 073901 (2018).
16. N. D. Hardy and J. H. Shapiro, "Reflective ghost imaging through turbulence," Phys. Rev. A **84**, 063824 (2011).
17. M. Bina, D. Magatti, M. Molteni, A. Gatti, L. A. Lugiato, and F. Ferri, "Backscattering differential ghost imaging in turbid media," Phys. Rev. Lett. **110**, 083901 (2013).
18. S. Feng, C. Kane, P. A. Lee, and A. D. Stone, "Correlations and fluctuations of coherent wave transmission through disordered media," Phys. Rev. Lett. **61**, 834–837 (1988).
19. M. J. Stephen and G. Cwilich, "Intensity correlation functions and fluctuations in light scattered from a random medium," Phys. Rev. Lett. **59**, 285–287 (1987).
20. M. C. W. van Rossum and T. M. Nieuwenhuizen, "Multiple scattering of classical waves: microscopy, mesoscopy and diffusion," Rev. Mod. Phys. **71**, 313–371 (1999).
21. A. U. Zyuzin and B. Z. Spivak, "Langevin description of mesoscopic fluctuations in disordered media," JETP Lett. **66**, 560–566 (1987).
22. R. Pnini and B. Shapiro, "Fluctuations in transmission of waves through disordered slabs," Phys. Rev. B **39**, 6986–6994 (1989).
23. M. van Albada, J. De Boer, and A. Lagendijk, "Observation of long-range intensity correlation in the transport of coherent light through a random medium," Phys. Rev. Lett. **64**, 2787–2790 (1990).
24. A. Z. Genack, N. Garcia, and W. Polkosnik, "Long-range intensity correlation in random media," Phys. Rev. Lett. **65**, 2129–2132 (1990).
25. J. F. de Boer, M. P. van Albada, and A. Lagendijk, "Transmission and intensity correlations in wave propagation through random media," Phys. Rev. B **45**, 658–666 (1992).
26. D. B. Rogozkin and M. Y. Cherkasov, "Long-range intensity correlations in wave reflection from a disordered medium," Phys. Rev. B **51**, 12256–12267 (1995).
27. L. Froufe-Perez, A. Garcia-Martin, G. Cwilich, and J. Sáenz, "Fluctuations and correlations in wave transport through complex media," Physica A **386**, 625–632 (2007).
28. T. Durduran, R. Choe, W. B. Baker, and A. G. Yodh, "Diffuse optics for tissue monitoring and tomography," Rep. Prog. Phys. **73**, 076701 (2010).
29. J. Bertolotti, E. van Putten, C. Blum, A. Lagendijk, W. Vos, and A. Mosk, "Non-invasive imaging through opaque scattering layers," Nature **491**, 232–234 (2012).
30. O. Katz, P. Heidmann, M. Fink, and S. Gigan, "Non-invasive single-shot imaging through scattering layers and around corners via speckle correlations," Nat. Photonics **8**, 784–790 (2014).
31. University of Exeter, Open Research Exeter (ORE), https://doi.org/10.24378/exe.1224.